

## Stellar iron abundances : non-LTE effects

F. Thévenin, T.P. Idiart

Observatoire de la Côte d'Azur

B.P. 4229,F-06304 Nice Cedex 4, France

Universidade de São Paulo, IAG, Depto. de Astronomia

C.P. 3386, São Paulo 01060-970, Brazil

Received \_\_\_\_\_; accepted \_\_\_\_\_

## ABSTRACT

We report new statistical equilibrium calculations for Fe I and Fe II in the atmosphere of Late-Type stars. We used atomic models for Fe I and Fe II having respectively 256 and 190 levels, as well as 2117 and 3443 radiative transitions. Photoionization cross-sections are from the Iron Project. These atomic models were used to investigate NLTE (non local thermodynamic equilibrium) effects in iron abundances of Late-Type stars with different atmospheric parameters. We found that most Fe I lines in metal-poor stars are formed in conditions far from LTE (local thermodynamic equilibrium). We derived metallicity corrections of about 0.3 dex with respect to LTE values, for the case of stars with  $[\text{Fe}/\text{H}] \sim -3.0$ . Fe II is found not to be affected by significant NLTE effects. The main NLTE effect invoked in the case of Fe I is overionization by ultraviolet radiation, thus classical ionization equilibrium is far to be satisfied. An important consequence is that surface gravities derived by LTE analysis are in error and should be corrected before final abundances corrections. This apparently solves the observed discrepancy between spectroscopic surface gravities derived by LTE analyses and those derived from Hipparcos parallaxes. A table of NLTE  $[\text{Fe}/\text{H}]$  and  $\log g$  values for a sample of metal-poor late-type stars is given.

*Subject headings:* NLTE effects — abundances — surface gravities

## 1. Introduction

Iron is a basic stone for the study of the chemical evolution of stellar systems. Relations between elemental abundance ratios  $[X/Fe]$  versus  $[Fe/H]$ <sup>1</sup> of giant and dwarf stars are generally used as tracers of chemical evolution of galaxies. The reason of this choice is that Fe lines are often quite numerous and easy to detect, even in very metal-poor stars. Hence, a good and precise determination of Fe abundances is of fundamental importance. Our understanding of Fe abundance in stars is mainly based on local thermodynamic equilibrium (LTE) analyses, for which many weak Fe I and Fe II lines are used. Most of the works devoted to spectral abundance analysis assume that the majority of these weak lines are not affected by important LTE deviations, in particular in the case of solar type dwarf stars. However, empirical studies of the ionization equilibrium of Fe I show some evidences that important NLTE (non local thermodynamic equilibrium) effects are suspected to be present in the photosphere of very metal-poor stars (Zhao & Magain 1990, Fuhrmann 1998, Feltzing & Gustafsson 1998). Calculations performed by Takeda (1991), which refers largely to other excellent computational works in the literature, imply in marginal NLTE effects on the ionization equilibrium for the giant star Arcturus and more important ones when removing the UV line opacities. NLTE effects were also investigated by Gigas (1986) in the hot star Vega, finding a correction of 0.3 dex for the iron abundance with respect to LTE value. Rutten (1988) and Steenbock & Holweger (1984) have also enlightened the problem, determining the most important NLTE mechanisms working in stellar atmospheres of Late-Type stars. If important corrections should have to be applied to LTE abundances, this could have a real importance on galactic chemical evolution models.

The basic theoretical problem of determination of stellar abundances through high

---

<sup>1</sup>X represents elements heavier than He

resolution spectral analysis is to solve the equation of radiation transfer, giving the variation of the radiative energy flow throughout an absorbing and emitting gaseous medium.

Firstly, the solution requires the construction of a stellar atmosphere model, which gives the thermodynamic variables, temperature  $T$  and pressure  $P$ , as a function of the optical depth  $\tau$ . Secondly, we have to determine the absorption and emission coefficients  $j_\nu$  and  $k_\nu$ , which are directly proportional to the transition probabilities and the number of atoms, ions or molecules in a given quantum state or energy level. Atomic, ionic and molecular populations depend on the elemental abundance and on the degree of excitation, ionization and dissociation respectively. These last quantities are calculated through the solution of the statistical equilibrium equations for given conditions of abundances, gas density, temperature, depending also on atomic and molecular constants. In a NLTE problem, elemental populations will depend, not only on gas temperature and density (as in LTE case), but also on the radiation field. To take this into account, we must analyze each line transition by considering the transitions of neighbouring levels and not as a two-level atom as in the LTE case. As a consequence, we have to calculate simultaneously the transfer and the statistical equilibrium equations for each considered level.

The real difficulty to treat a complete iron atom in the NLTE case, is to solve the statistical equilibrium equations including about 300 terms and 5000 multiplets. The diagnostic concerns a lot of strong UV lines, a lot of optical lines (as is used in classical detailed analysis), and also a lot of infrared lines which come from the highest terms of the atomic model, i.e., those with an excitation potential greater than 3 eV. We present in this work a much more complex model for Fe I and Fe II, taking into account a larger number of levels and transitions than those found previously in the literature. Our main goal is to estimate NLTE effects in the determination of Fe abundances using the curve of growth technique, as in a classical LTE analysis. In addition, this procedure allow us to check the ionization equilibrium and, consequently, to evaluate NLTE effects in the  $\log g$

determination.

In section 2 we present our atomic models and the strategy to correct Fe abundances, and in addition surface gravities, of NLTE effects. In sections 3 and 4 we discuss the results for the Sun and stars previously studied in other works, respectively. In section 5, our results for metal-poor stars are given, and in section 6 we present our conclusions and some suggestions for future stellar abundance analyses.

## 2. The iron atom model and the strategy

### 2.1. Fe I and Fe II atoms

Our first step for the analysis of NLTE effects was the elaboration of Fe I and Fe II atomic models. Our goal was to construct the best models from the statistical point of view, taking into account a complete set of levels and transitions. We have not tried to produce synthetic spectra to compare to observed profiles, but to give differential abundance corrections using equivalent widths and curves of growth, as will be described later in section 3.

For Fe I and Fe II we consider levels with principal quantum numbers  $n=1,3,5, 7$  and  $n=2,4,6,8$  respectively. For computing time reasons we restricted our Fe I /Fe II models to 256/190 levels, having a potential less than 6.8/8.7 eV and a continuum at 7.90/16.1 eV. In both models, fine structure were taken into account, resulting in a total of 2117 radiative transitions for Fe I and 3443 for Fe II. We have not considered line transitions in the far infrared ( $\lambda > 5.0\mu m$ ). Grotrian diagrams of our Fe I and Fe II models are given in Fig. 1.

The code used to solve the equations of statistical equilibrium and radiative transfer is MULTI, described by Carlson (1986), which use the operator perturbation technique of Scharmer & Carlsson (1985). We used version 2.2 (1995). Radiation fields for each

stellar atmospheric model are computed using opacities from Uppsala package, including effects of some line blanketing. We did not use the option of the code which produces NLTE background opacities, once the models of atmospheres used here are based on LTE calculations (see 2.2) and our results do not have such degree of precision for individual line profiles yet (see section 3). As stated above, we are interested in the derivation of differential abundance corrections based on a curves of growth analysis. A better treatment of the opacity would be its derivation with the same code used to compute the atmospheric model, however, such treatment would probably not change strongly our results, mainly for metal-poor stars.

Input atomic data for this code are:

a) Energy levels:

- excitation potentials
- statistical weights
- ionization stages

b) Transitions:

- oscillator strengths
- radiative and collisional damping coefficients
- photoionization cross-sections
- excitation and ionization collisional cross-sections.

Excitation potentials of the levels and their statistical weights are given by Hirata & Horaguchi's table (1995). For radiative transitions we used oscillator strengths given

by Fuhr, Martin & Wiese (1988), Hirata & Horaguchi (1995) and Thévenin (1989, 1990). Damping coefficients are used for calculation of line profiles (line broadening). The total line damping coefficient is given by  $\gamma = \gamma_{\text{rad}} + \gamma_{\text{coll}}$ , where  $\gamma_{\text{rad}}$  and  $\gamma_{\text{coll}}$  are respectively the radiative and collisional damping coefficients. Radiative or natural damping width is defined as :  $\gamma_{\text{rad}} = \sum_{l < i} (A_{il}) + \sum_{l < j} (A_{jl})$  where  $A_{il}$  are the Einstein coefficients. The collisional damping coefficient is the sum of van der Waals and Stark coefficients, which take into account effects due to perturbations with neutral H and He (van der Waals) and charged particles (Stark). For all lines the classical van der Waals damping is evaluated from the classical approximation (Unsöld 1955) and multiplied by an enhancement factor, since van der Waals constant cannot reproduce the real lines profiles (see Gurtovenko & Kostic 1982, Thévenin 1989 or more recently Anstee, O'Mara & Ross 1997), which will be discussed in section 3. In our case, damping due to Stark effect can be neglected, because the electronic density in the photosphere of the Late-Type stars investigated here is much smaller than neutral H density.

Photoionization for all levels of Fe I and Fe II was treated in details by using the frequency dependence of the cross-sections given by the Iron Project (Bautista 1997). At each layer of the star's photosphere models ionizing radiation fields are computed, giving an estimate of photoionization rates. Note that if the ionization equilibrium is not achieved, the opacity computed would have to be changed by changing the iron abundance. The very detailed cross-sections given by the Iron Project were smoothed to decrease the number of points in tables cross-section vs. frequency for each level, in order to reduce the computing time. It was easy to check on some levels that this smoothing of the detailed cross-sections had no consequences on the final results of the radiative transfer computations. But, for some of the levels, when strong resonances in the photoionization cross-sections near the threshold exist, details were considered.

Collisional ionization rates with electrons are derived from the approximate formulae given by Mihalas (1978). For the evaluation of collisional rates of permitted transition lines we used van Regemorter's formulae (1962). For some forbidden lines considered, collisional rates were derived from the formulae of Auer & Mihalas (1973) with  $\Omega=0.1$ , not equal to 1.0 as proposed by Takeda (3.1.2, 1991)(see Cayrel et al. 1996). However, these forbidden lines seem to play a negligible role in our Fe models. Uncertainties in the collisional processes with neutral H and He are probably the main source of errors in our models. The lack of accurate cross-sections for collisions with hydrogen atoms is largely discussed in the recent literature. The use of the Drawin's theory (1968, 1969), as proposed by Steenbock & Holweger (1984), was severely criticized by Severino, Caccin & Gomez (1993), estimating that Drawin's theory gives cross-section values larger by a factor of  $10^3$  for NaD lines. A clear sum-up of the situation is given by Holweger (1996). In the absence of a more precise theory we used this approach as already done in many other works. But, we emphasize that we found globally no important consequences on the population distribution in atomic levels and therefore on the equivalent width of lines transitions of our Fe I and Fe II models, when using or not hydrogen collisions.

We notice that changing Bautista's photoionization cross-section values by a factor 2 induces changes in the resulting populations, giving errors on  $[\text{FeI}/\text{FeII}]$  less than 0.02 dex. This means that our strategy developed around the technique of the curve of growth (see 2.3) has a low dependence on such atomic parameters. Of course this is not true if profiles of Fe lines are used to perform the stellar chemical abundance analyses.

## 2.2. The atmospheric models

In order to investigate NLTE effects on the ionization balance of iron with different stellar atmospheric parameters, atmosphere models for different known stars were generated

using the Bell et al. (1976) grid. This grid was used to be self-consistent with Thévenin's catalogue (1998), which reanalyzes LTE abundances of 35 chemical elements for 1107 stars. These models reproduce well the atmosphere of Pop II F to K dwarfs and giants, for which LTE atmospheric parameters were taken from Thévenin's catalogue. Microturbulent velocities were taken independent of the optical depth. No macroturbulent velocity was used in our computations.

We have check that Bell et al.'s models (1976) and Kurucz's models (1993) for a dwarf metal-poor star give no significant differences on results of [FeI/FeII].

The solar iron abundance adopted in this work is  $A_{Fe} = 7.46^2$  (Holweger 1979) as also used by Thévenin (1998). The reason of this choice is clearly explained in Thévenin (1989, see discussion & Table III). Other determinations have lead to similar solar abundances (see for example Holweger, Heise & Kock 1990 or Holweger et al. 1991).

### 2.3. The strategy to estimate NLTE effects

To compute NLTE effects on the derived LTE surface gravities and [Fe/H] values, we constructed NLTE curves of growth for both Fe I and Fe II, using the equivalent widths  $W$  calculated with MULTI for a given stellar atmospheric model and for all transitions considered, as a simulation of observed equivalent widths. The abscissae of the curves of growth are computed under the condition of LTE as classically done by detailed analysis, for each of the 2117 Fe I and 3445 Fe II lines. However, to fit the classical LTE curves of growth for each analyzed star, we used only lines ranging between  $\lambda\lambda 2200-10000$  Å to be consistent with classical detailed analysis procedure. Once that atmospheric parameters estimated for a given star are from LTE analysis (see Table 2, Thévenin 1998), we can

---

<sup>2</sup> $A_{Fe} = \log(N_{Fe}/N_H) + 12.0$

immediately check the validity of this assumption and correct, if necessary, LTE values of [Fe/H] in the same table. But, before to correct the metallicities, we have to check the ionization equilibrium to derive the error on  $\log g$  due to NLTE effects. If [FeI/H] were not equal to [FeII/H], this would mean that the classical LTE detailed analysis is wrong and would have forced the ionization equilibrium using a wrong surface gravity. Hence, for all stars, we had to calculate theoretical curves of growth with new corrected values of  $\log g$  and then estimate metallicity corrections.

### 3. Results in the solar case

For the Sun, we used a model from the grid of Bell et al. (1976) given by Gustafsson (1981) and, in addition, tested the Holweger-Müller's model (1974) to compare the results of both models for profiles of strong lines. We used the same solar abundance 7.46 for both models. Defining  $W_{\text{NLTE}}$  and  $W_{\text{LTE}}$  as the computed equivalent width in NLTE and LTE conditions respectively, results of  $W_{\text{NLTE}}/W_{\text{LTE}}$  ratios, which give the importance of NLTE effects on each spectral line, differ but not considerably from one model to other. However, these two models give differences on the profile of strong lines like  $\lambda 4045 \text{ \AA}$  (see Fig. 2). The enhancement factor of the  $\gamma_H$  van der Waals constant has to be 2.5 for Holweger-Müller's model and only 1.3 when one uses the Gustafsson's model, to fit perfectly the profiles by Kurucz et al. (1984). The value of 2.5 is classical and universally adopted for most of the lines, but it can vary from one line to another. This problem has been treated by Anstee, O'Mara & Ross (1997) who reproduce well enhancement factors ranging from 1.4 to 3.3. Once that for late-type stars analysis we used the Bell et al.'s grid of models, we decided to keep the value of 1.3 for all radiative transition lines of our Fe I and Fe II models, since we do not try to reproduce perfectly all the line profiles. This problem was also found for the Ca I triplet lines (e.g. Cayrel et al. 1996), where Gustafsson's model looks less good

when using a theoretical enhancement factor of 2.44 for the Ca I line  $\lambda$  6162 Å, compared to the result obtained with the Holweger-Müller's model. This of course has an important consequence on detailed analysis of very metal-poor stars, because these strong lines would have to be used once that they are the only ones measurable on observed spectra.

For solar photosphere, there were no important NLTE effects (overionization around 0.02 dex) found by the position of the curves of growth of Fe I and Fe II. Once the precision of curve of growth's fit is around 0.04 dex, we have adopted 0.0 dex NLTE effect for Gustafsson's solar model. Consequently, one can say that the ionization equilibrium is perfectly reproduced by the LTE surface gravity  $\log g_{\odot} = 4.44$ . This absence of overionisation is due to important UV line blocking in solar dwarf stars and is independent of the solar model used. Fig. 3 shows the solar theoretical curves of growth of Fe I and Fe II considering only computed lines ranging between  $\lambda\lambda$  2200 - 10000 Å (see section 2.3). As we can see, curves of growth have a thickness which is produced by small NLTE effects giving an increase or a decrease of  $W$ , depending on population of levels from which lines are formed - e.g. depending on the excitation potential (see also Holweger 1996). These effects can be seen by the analysys of each line profile, whose detailed study is not the purpose of this paper, as mentioned in section 2.1. Our interest is centered in the problem of overionization, which have direct consequences on the ionization equilibrium (not in NLTE effects in line profiles) and therefore on curve of growth analysis.

In 1949, Carter was the first to point out that the solar curve of growth in its damping part is divided into two main branches. Different conclusions were proposed to interpret it: the odd-even effect, the dependence of the damping constant on the multiplet of the lines (Carter 1949, Cayrel de Strobel 1966, Pagel 1965), but no comprehensible solutions were demonstrated (Foy 1972). Rutten & Zwaan (1983) had suspected NLTE effects. Usually neglected, this effect had no disastrous consequences on curve of growth analysis, because

the lines used to determine stellar abundances were not strong enough to lie in the damping part where this effect exists. Fig. 3 shows clearly double branches in the damping part for Fe I and Fe II. We remarked that the lower branch of damping curve of, for example, Fe I refers to lines originated from the ground levels (5D). The upper part is populated by lines originated from the (5F), which can be considered as resonance levels, because there are no permitted transitions with the ground level (5D). It seems that these 5D levels are pumped toward upper levels with more efficiency than the next levels (5F). UV lines clearly pump these levels as shown on Fig. 4, where  $b_i = n_i^{\text{NLTE}}/n_i^{\text{LTE}}$  is the classical coefficient used to study NLTE effect. In these two levels,  $b_i$  have respectively values close to 0.13 and 0.24. Damping lines vary as the square of abundance, which means that for two lines having the same abscissae ( $\log X$ ) the ratio of their  $W_{\text{NLTE}}$  is varying as the square of  $b_i/b_j$ , i.e. 0.14 as can be checked on Fig. 3. This amplitude of the double branching of the Carter's effect is of the same order of magnitude as found on empirical solar iron curve of growth. We drawn attention to spectroscopists using lines originated from these Fe I resonance levels to be careful before deriving stellar iron abundances for very metal-poor stars, for which these lines are the only one easily measurable. Fe II lines present the same effects of splitting, but NLTE effects (see Fig. 4) are globally less pronounced, because they are formed in deeper parts of the photosphere. However, Anstee, O'Mara & Ross (1997) proposed a new approach of the theory of damping constant which could help to understand Carter's effect. Probably more detailed and precise computations are needed to determine the contribution of both results in Carter's effect.

#### 4. Comparison with other works

Before to compute numerous new NLTE surface gravities  $\log g$  and  $[\text{Fe}/\text{H}]$  for metal-poor stars, we decided to compare our technique predictions for two stars previously

studied by other authors. One is Arcturus (Takeda 1991) and the other is Vega (Gigas 1986). In the case of the cool giant metal-poor star Arcturus we found negligible NETL effects of the same order as computed by Takeda: 0.03 and -0.02 respectively for Fe I and Fe II. For the hot star Vega, significant NLTE effects were derived. Because NLTE corrections on abundances of Fe I and Fe II were not the same, ionization equilibrium was not satisfied by the input of LTE surface gravity. We had to iterate until reach the following values for Vega :  $\log g_{\text{Vega}} = 4.29$ ,  $[\text{Fe}/\text{H}]_{\text{Vega}} = -0.33$  ( $A_{\odot} = 7.46$ ). This iron abundance is comparable to that of Gigas (1986), who proposed -0.55 dex (using a solar reference value of 7.67). It should be noted that most of Fe I lines are formed around  $\log \tau \sim -1. - 2.$ , on the contrary Fe II lines are generally formed in deeper parts of atmospheres.

## 5. Results on metal-poor subgiant to subdwarf stars and consequences

We selected in Thévenin's catalogue a set of 136 subgiant to subdwarf stars, with abundances ranging between -4.0 and 0.0 dex. We applied our strategy described in section 2.3 to each of them. Results are presented in table 1. As one check of our final results, we compare computed  $W_{\text{NLTE}}$  for Fe I and Fe II lines for the metal poor star HD 140283 with those measured by Ryan, Norris & Bessel (1991). The correlation is shown on Fig. 7. One can note that Fe I and Fe II lines are mixed, meaning that the estimated value  $\log g = 3.74$  is correct - same conclusion for  $[\text{Fe}/\text{H}] = -2.21$ . Its surface gravity was changed from giant to subgiant as derived by Hipparcos parallax ( $\log g = 3.79$ , Nissen, Høg & Schuster (1997)). We show on Fig. 5 and Fig. 6 the amplitude of the overionization in the atmosphere of HD 140283 analyzed with the LTE atmospheric parameters.

Nissen et al. (1997) have shown that exists a discrepancy between spectroscopic  $\log g$  taken in the litterature and those deduced from Hipparcos parallaxes. On Fig. 8 are plotted the  $\log g_{\text{NLTE}}$  values derived by us versus  $\log g$  Hipparcos (Nissen et al. 1997 and Clementini

et al. 1998) for stars in common, showing that our results are remarkably close to those from Hipparcos. Among the four points having the worst correlation (Nissen et al.'s values), two stars are suspected to be double. The adopted error bars are those of Nissen et al. (1997), Clementini et al. (1998) and Thévenin (1998).

Overionization by UV lines seems to play an important role in stellar atmospheres of poor Late-Type stars. As can be seen on Fig. 6,  $b_i$  Fe I coefficients are for most of the levels far below 1.0, increasing from resonance levels to upper levels until  $\sim 1.2$  - upper levels are concerned by infra-red transitions. In consequence, the source function  $S_\nu \approx b_j/b_i \times B_\nu$  satisfies the relation  $S_\nu > B_\nu$  for most of UV transitions (where  $B_\nu$  is the Planck function). Also for strong resonance lines the mean intensity satisfies the relation  $J_\nu > B_\nu$  and drain lower levels towards upper levels, which are more easily ionized. Consequently, upper levels are overpopulated,  $J_\nu$  decreases far below the Planck function and produces infrared recombinations. These important mechanisms are well explained in Bruls, Rutten & Shchukina (1992) and we refer to this paper for more details.

The results for our sample of stars are :

- If  $T_{\text{eff}}$  increases, UV radiation field and the pumping of the resonance levels increase, but the infrared radiation field decreases too and the overionization do not increase as it would be expected.
- If  $T_{\text{eff}}$  decreases, infrared radiation increases and are more efficient to overionize the upper levels. The effect of  $T_{\text{eff}}$  variations on the overionization for F to G stars is found to be not very pronounced.
- If abundance decreases, UV line blocking decreases rapidly and the overionization becomes very important as shown on the relation between metallicity correction factors  $\Delta_{[\text{Fe}/\text{H}]}$  and metallicities estimated by LTE approach (Fig. 9). This reveals that the

overionisation increases rapidly when the abundance decreases from  $\approx -0.3$  to  $-1.5$  dex to reach a maximum for metal-poor stars having  $[\text{Fe}/\text{H}] \approx -3.0$ . There are no significant overionization for solar type stars.

The most important parameter to produce overionization, the main source of NLTE effects on curves of growth technique, is therefore the variation of metal abundance in atmospheres of Late-Type stars.

The precision of  $[\text{FeI}/\text{H}]$  or  $[\text{FeII}/\text{H}]$  determination by using theoretical curves of growth is estimated to be 0.04 dex, as mentioned in section 3, meaning that corrections on  $\log g$  reach a precision of 0.08 dex.

We computed Fe I and Fe II curves of growth for hot supergiant star parameters corresponding to stars analysed in the Magellanic Clouds. These stars have moderate underabundances ( $\sim -0.6$  to  $-0.2$ ) dex. We found a  $[\text{FeI}/\text{FeII}]$  balance between 0.05 and 0.01 dex for SMC stars (see stellar parameters in Thévenin 1998). Holweger (1990) mentioned that iron NLTE effects computed using the LTE atmospheric parameters of the poor giant star  $CD - 38^{\circ}245$  lead to an error in the ionization equilibrium balance of +0.3 dex, value very similar to those derived by us for dwarfs stars. These results are not surprising as mentioned by Feltzing & Gustafsson (1998), once the UV opacity increases with the increase of the Balmer lines when the surface gravity decreases. This only means that the idea that NLTE deviations must necessarily increase with the decrease of surface gravities (hence increase in collisions) is not entirely correct. From the point of view of Boltzmann's law this is true, but if the UV flux is blocked by increasing of Balmer lines, deviation from the point of view of Saha's law do not increase with  $\log g$  decreasing.

## 6. Conclusion

We presented a study of departures from LTE for Fe I and Fe II, mostly for metal-poor stars. The mechanism of these departure is clearly identified as overionisation, responsible for important corrections on the values of surface gravities. A good correlation between our derived surface gravities and those deduced from Hipparcos parallaxes is a proof of the validity of our results in table 1, having important consequences on distances in the Galaxy. These corrections on the surface gravity could have also important incidences on the abundances of elements like Be (Gilmore, Edvardsson & Nissen 1991). NLTE abundance corrections are found to be less than 0.35 dex, but not negligible. Therefore, stellar abundance ratios could have to be revisited after having estimated possible NLTE effect on other elements like Ca, Mg, Al, O and Be. We are preparing papers on these subjects. We recommend to stellar spectroscopists working on metal-poor stars to use NLTE computations or the table 1 before to publish their LTE results, or to use surface gravities derived by Hipparcos parallaxes combined with a LTE analysis of Fe II lines which do not suffer important NLTE effects.

We wish to thank M. Bautista for having provided his photoionization cross-sections prior to publication and R. Cayrel, J.A. de Freitas Pacheco, R. Gratton, F. Paletou, J. Tully and Cl. Van t' veer for fruitful discussions. This work was facilitated by the use of the SIMBAD database, operated by the Centre de Données astronomiques de Strasbourg (CDS - France) and has been performed using the computing facilities provided by the program *Simulations Interactives et Visualisation en Astronomie et Mécanique (SIVAM)* at the computer center of the Observatoire de la Côte d'Azur.

T.I. acknowledges the brazilian agencies CNPq for the post-doctoral fellowship 201249/95-2 at the Observatoire de la Côte d'Azur during the years 1996-97, and FAPESP

for the present post-doc grant 97/13083-7 at IAG. F.T. thanks FAPESP for the grant 98/10869-2 at IAG.

## REFERENCES

Anstee S.D., O'Mara B.J., Ross, 1997, MNRAS 284, 202

Auer L.H., Mihalas D. 1973, ApJ, 184, 151

Bautista M.A. 1997, A&AS, 122, 167

Bell R.A., Ericksson K., Gustafsson B., Nordlund Å 1976, A&AS, 23, 37

Bruls J.H.M.J., Rutten R.J., Shchukina N.G. 1992, A&A, 265, 237

Carlsson M. 1986, Uppsala Astronomical Observatory Report 33

Carter W.W. 1949, Phys. Rev., 76, 962

Cayrel R., Faurobert-Scholl M., Feautrier N., Spielfiedel A., Thévenin F. 1996, A&A 312, 549

Cayrel, Jugaku, J. 1963, Ann. Astrophys. 26, 495

Cayrel de Strobel G. 1966, Ann. Astrophys., 29, 413

Clementini G., Gratton R.G., Carretta E., Sneden C. 1998, Mon.Not.R.Astron. Soc., in press, astro-ph/9808298

Drawin H.W. 1968, Z.Physik, 211, 404

Drawin H.W. 1969, Z.Physik, 225, 483

Feltzing S., Gustafsson B. 1998, A&A, 129, 237

Foy R. 1972, A&A, 18, 26

Fuhr, J.R., Martin, G.A., Wiese, W.L. 1988, in *Atomic transition probabilities. Iron through Nickel*, New York: American Institute of Physics (AIP) and American Chemical Society

Fuhrmann K. 1998, A&A, 330, 626

Gigas D. 1986, A&A, 165, 170

Gilmore G., Edvardsson B., Nissen, P.E. 1991, ApJ, 378, 17

Gurtovenko E.A., Kostic R.I. 1981, A&AS, 46, 239

Gustafsson B. 1981, Private communication.

Hirata R., Horaguchi T. 1995, CDS, Catalogue VI/69

Holweger H. 1979, *Les éléments dans l'Univers*, Proceeding 22nd Liège Intern. Astrophys. Colloquium, Université de Liège, p117

Holweger H. 1990, private communication of a work done with Steenbock and Bessel.

Holweger H. 1996, Physica Scripta T65, 151

Holweger H., Heise C., Kock M. 1990, A&A, 232, 510

Holweger H., Bard A., Kock A., Kock M. 1991, A&A, 259, 545

Holweger H., Müller Ed. 1974, Sol. Phys., 39, 19

Kurucz R.L., Furenhild I., Brault J., Testerman L. 1984, National Solar Observatory, Atlas N. 1

Kurucz R.L. 1993, CDrom 13

Mihalas D. 1978, *Stellar atmospheres* 2nd ed., W.H. Freeman, San Francisco, p134

Nissen P.E., Gustafsson B., Edvardsson B., Gilmore G. 1994, A&A, 285, 440

Nissen P.E., Høg E., Schuster W.J. 1997, HIPPARCOS Venice '97 Symposium ESA SP-402

Pagel B.E.J. 1965, R. Obs. Bull., 104

van Regemorter H. 1962, ApJ, 136, 906

Ryan G.S., Norris J.E., Bessell M.S. AJ, 102, 303

Rutten R.J. 1988, in *Physics of formation of Fe II outside LTE*, Proceedings of the 94<sup>o</sup> IAU Colloquium, Anacapri, Italy, Dordrecht, D. Reidel Publishing Co., p. 185

Rutten R.J., Zwaan C 1983, A&A, 117, 21

Scharmer G.B., Carlsson M. 1985, J. Comp. Phys., 59, 56

Severino G., Caccin B., Gomez M.T. 1993, Mem.Soc.Astron.Ital., 64-3, 565

Steenbock W., Holweger H. 1984, A&A, 130, 319

Takeda Y. 1991, A&A, 242, 455

Thévenin F. 1989, A&AS, 77, 137

Thévenin F. 1990, A&AS, 82, 179

Thévenin F. 1998, CDS Information Bulletin n=49, in press, catalog n=III/193

Unsöld A 1955, Physik der Sternatmospheren, Berlin : Springer

Zhao G., Magain P. 1990, A&A, 238, 242

Fig. 1.— Grotrian diagrams for Fe I and Fe II atoms. Each configuration term is denoted by an alphabetic notation, representing the degeneracy of the state. Two Fe II levels do not have configuration terms identified, then they were labeled 62065 and 65363 (which refers to line transitions  $\lambda\lambda$  6206.5 and 6536.3 Å) as Hirata & Horaguchi's table.

Fig. 2.— Comparison between two calculated Fe I NLTE line profiles and observed spectra for the sun. The theoretical profiles were calculated using the atmospheric models of Holweger-Müller (1974) and Gustafsson (1981), for different enhancement factors  $f_H$  of the van der Waals constant. Observed spectra are from Kurucz et al. (1984).

Fig. 3.— Theoretical Fe I and Fe II curves of growth for the sun.  $\log X = \log gf + \log \Gamma + \log(N_{\text{Fe}}/N_{\text{H}})$ , where  $gf$  is the oscillator strength;  $\Gamma$  is a parameter defined for each line as a function of the atmospheric model (Cayrel & Jugaku 1963);  $N_{\text{Fe}}/N_{\text{H}}$  is the relative abundance.

Fig. 4.— Departure coefficients of Fe I and Fe II versus optical depth in the solar case.  $b_i = n_i^{\text{NLTE}}/n_i^{\text{LTE}}$ , where  $n_i^{\text{NLTE}}$  and  $n_i^{\text{LTE}}$  are NLTE and LTE populations respectively for each level.

Fig. 5.— Theoretical Fe I and Fe II curves of growth for the star HD 140283, computed with LTE atmospheric parameters:  $\theta_{\text{eff}}=0.90$ ,  $\log g = 3.20$  and  $[\text{Fe}/\text{H}]=-2.5$ . For Fe I is overplotted the classical LTE curve of growth (full line), showing the need of correction by NLTE effects.

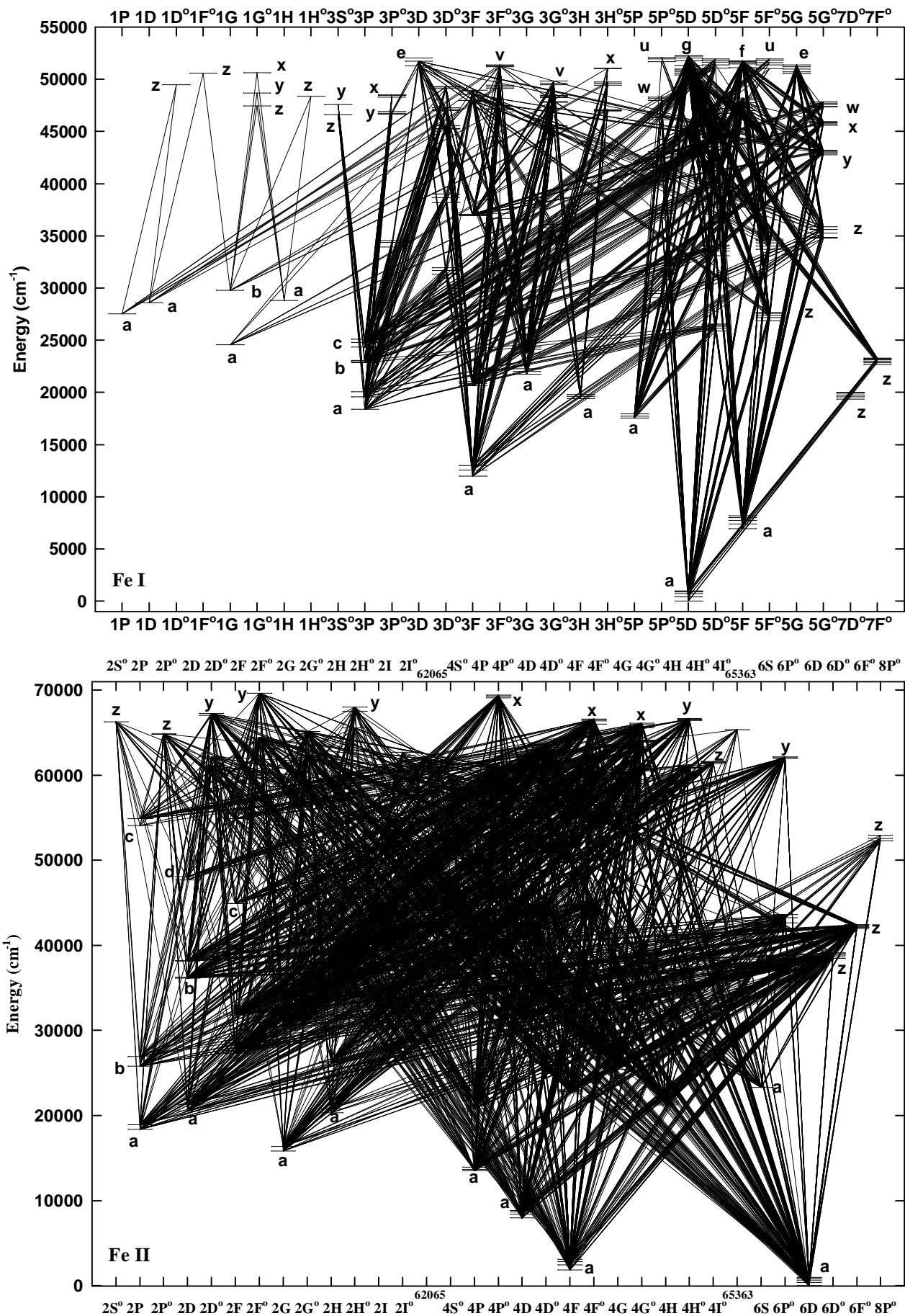
Fig. 6.— Departure coefficients of Fe I versus optical depth for HD 140283 ( $\theta_{\text{eff}}=0.90$ ,  $\log g = 3.20$  and  $[\text{Fe}/\text{H}]=-2.5$ ).  $b_i = n_i^{\text{NLTE}}/n_i^{\text{LTE}}$ , where  $n_i^{\text{NLTE}}$  and  $n_i^{\text{LTE}}$  are NLTE and LTE populations respectively for each level.

Fig. 7.— Computed equivalent widths for Fe I and Fe II lines versus observed ones by Ryan

et al. (1991) for Fe I and Fe II for HD 140283. Atmospheric parameters for calculation of equivalent widths are corrected of NLTE effects.

Fig. 8.— Comparison between our derived  $\log g$  and those using Hipparcos distances from Nissen et al. (1997) and Clementini et al. (1998).  $\log g_{\text{NLTE}}$  error bars are estimated from classical detailed analysis for dwarf stars  $\sim 0.30$  dex (Thévenin 1998).

Fig. 9.— Final estimated NLTE abundance corrections  $\Delta_{[\text{Fe}/\text{H}]}$  versus LTE atmospheric parameters from Thévenin (1998).



## FIGURE 1

TABLE 1  
NETL RESULTS FOR 136 STARS

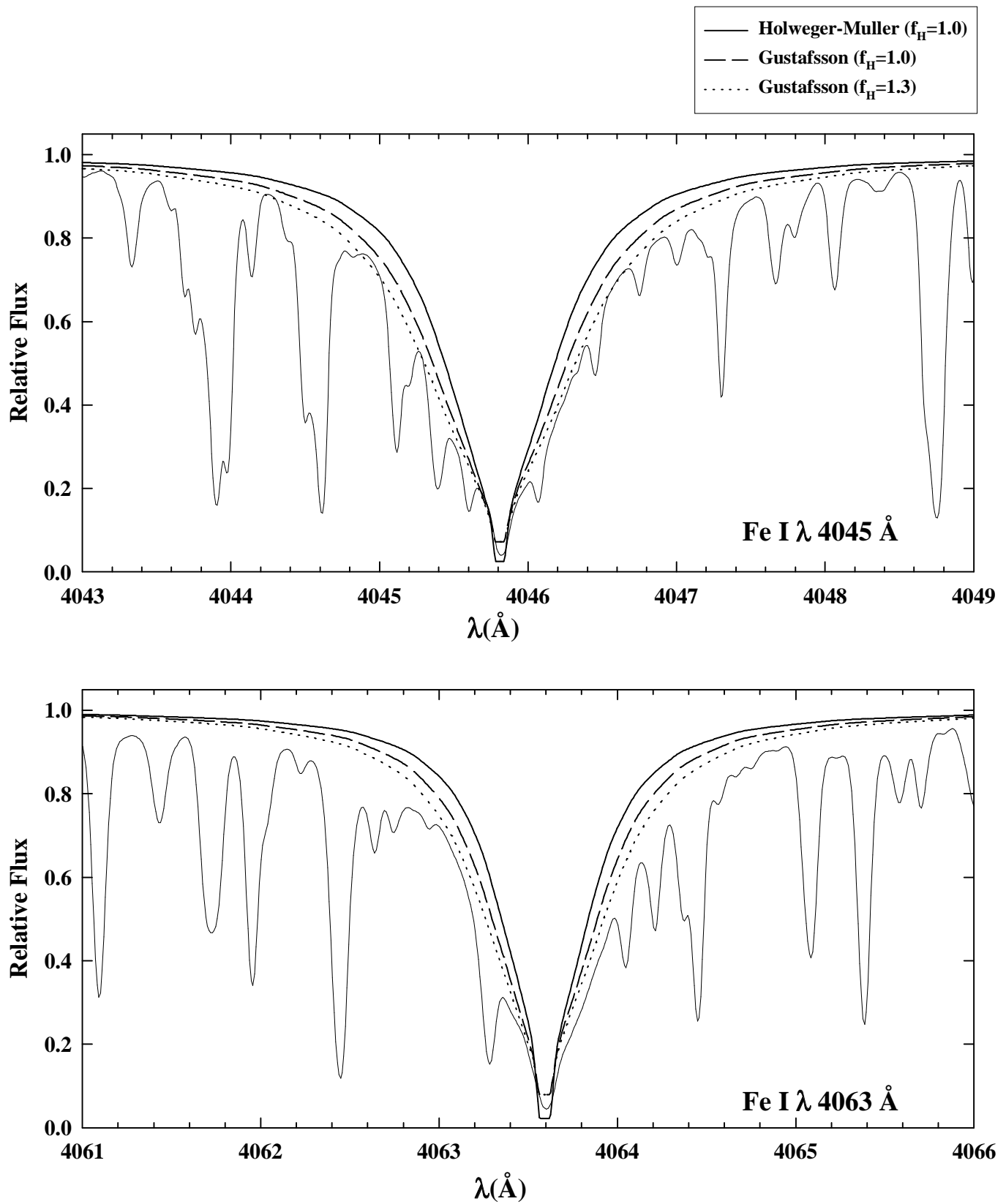
Star	$\Theta_{eff}$	$log g_{(ETL)}$	$v_{turb}(\text{km.s}^{-1})$	$[\text{Fe}/\text{H}]_{(ETL)}$	$[\text{Fe}/\text{H}]_{(\text{NETL})}$	$log g_{(\text{NETL})}$
HD 26	0.96	2.50	1.3	-0.35	-0.29	2.59
HD 400	0.81	4.10	1.0	-0.22	-0.15	4.21
HD 739	0.77	4.30	1.2	-0.02	-0.02	4.32
HD 2454	0.78	4.10	1.0	-0.26	-0.21	4.17
HD 2615	0.81	3.90	1.0	-0.53	-0.45	4.01
HD 3567	0.84	3.90	1.2	-1.25	-1.05	4.21
HD 6434	0.87	4.40	1.0	-0.48	-0.38	4.51
HD 6582	0.95	4.50	1.0	-0.70	-0.56	4.67
HD 7439	0.78	4.10	1.0	-0.22	-0.19	4.16
HD 13555	0.79	4.10	1.2	-0.22	-0.19	4.14
HD 16031	0.84	3.80	1.1	-1.82	-1.56	4.14
HD 16895	0.80	4.30	1.1	0.08	0.08	4.30
HD 17548	0.84	4.30	1.0	-0.50	-0.43	4.41
HD 19445	0.86	4.00	1.4	-2.10	-1.88	4.42
HD 23439A	1.01	4.30	1.0	-0.97	-0.85	4.53
HD 23439B	1.06	4.20	1.0	-1.05	-0.86	4.46
HD 25329	1.04	4.50	1.0	-1.75	-1.67	4.73
HD 25704	0.86	4.20	1.1	-0.75	-0.64	4.28
HD 30649	0.88	4.20	1.0	-0.48	-0.40	4.31
HD 34328	0.84	4.10	1.2	-1.65	-1.42	4.41
HD 43947	0.85	4.30	1.0	-0.22	-0.19	4.35
HD 48565	0.85	3.50	1.0	-0.65	-0.54	3.72
HD 48938	0.83	4.20	1.0	-0.31	-0.26	4.28
HD 51530	0.84	3.90	1.0	-0.45	-0.38	3.99
HD 58551	0.82	4.20	1.2	-0.45	-0.40	4.31
HD 59392	0.84	3.60	1.2	-1.65	-1.44	3.96
HD 59984	0.84	4.20	1.0	-0.66	-0.52	4.44
HD 61421	0.76	4.00	1.7	0.05	0.05	4.00
HD 63077	0.88	4.10	1.0	-0.70	-0.53	4.36
HD 64090	0.94	4.20	1.2	-1.75	-1.52	4.54
HD 68284	0.86	3.95	1.0	-0.50	-0.41	4.11
HD 69611	0.87	4.30	1.0	-0.50	-0.40	4.45
HD 69897	0.79	4.40	1.0	-0.15	-0.12	4.44
HD 74000	0.82	3.90	1.4	-2.10	-1.83	4.25
HD 74011	0.88	4.20	1.0	-0.60	-0.46	4.42
HD 76932	0.86	3.50	1.0	-0.90	-0.79	3.75
HD 81809	0.90	3.80	0.6	-0.35	-0.27	3.92
HD 82328	0.79	4.20	1.2	-0.06	-0.05	4.23
HD 84937	0.81	3.90	1.3	-2.10	-1.86	4.27
HD 89707	0.84	4.40	1.0	-0.35	-0.28	4.49
HD 94028	0.85	4.10	1.2	-1.50	-1.31	4.39
HD 97916	0.82	3.90	1.2	-1.00	-0.86	4.11
HD 98553	0.85	4.40	1.0	-0.35	-0.28	4.50
HD 99383	0.85	3.80	1.6	-1.60	-1.36	4.17
HD 103095	1.01	4.50	1.2	-1.35	-1.19	4.77
HD 107113	0.79	4.10	1.2	-0.40	-0.35	4.20
HD 108177	0.84	4.00	1.0	-1.70	-1.51	4.37
HD 110897	0.86	4.30	1.0	-0.45	-0.37	4.41

TABLE 1—Continued

Star	$\Theta_{eff}$	$log g_{(ETL)}$	$v_{turb}(\text{km.s}^{-1})$	$[\text{Fe}/\text{H}]_{(ETL)}$	$[\text{Fe}/\text{H}]_{(\text{NETL})}$	$log g_{(\text{NETL})}$
HD 113226	1.01	2.70	1.6	0.11	0.13	2.74
HD 114762	0.87	4.00	1.0	-0.72	-0.56	4.24
HD 114837	0.80	4.30	1.0	-0.22	-0.18	4.37
HD 116064	0.86	3.70	1.4	-2.10	-1.87	4.08
HD 124897	1.16	2.00	1.5	-0.40	-0.37	2.05
HD 130551	0.81	4.20	1.0	-0.55	-0.48	4.32
HD 132475	0.92	3.50	0.8	-1.62	-1.37	3.88
HD 134169	0.87	3.80	1.0	-0.87	-0.68	4.06
HD 134439	1.01	4.40	1.0	-1.50	-1.31	4.73
HD 140283	0.90	3.20	1.4	-2.50	-2.21	3.74
HD 142373	0.86	4.00	1.1	-0.40	-0.27	4.24
HD 144172	0.80	4.10	1.0	-0.38	-0.35	4.21
HD 147609	0.80	3.50	1.2	-0.38	-0.36	3.61
HD 148211	0.85	4.20	1.0	-0.59	-0.47	4.38
HD 148816	0.86	4.10	1.0	-0.65	-0.51	4.32
HD 149414	1.01	4.00	1.2	-1.30	-1.08	4.34
HD 150177	0.81	3.90	1.2	-0.48	-0.40	4.00
HD 150453	0.78	3.90	1.0	-0.27	-0.22	3.98
HD 155358	0.86	4.10	1.0	-0.60	-0.47	4.28
HD 155886	0.98	4.60	1.0	-0.25	-0.24	4.60
HD 156026	1.11	4.60	1.0	-0.25	-0.21	4.67
HD 157089	0.87	4.10	1.0	-0.48	-0.39	4.24
HD 157214	0.89	4.30	1.0	-0.35	-0.32	4.36
HD 159307	0.81	3.90	1.0	-0.64	-0.54	4.03
HD 160617	0.85	3.50	1.6	-1.75	-1.48	3.84
HD 160693	0.88	4.00	1.0	-0.65	-0.52	4.21
HD 160933	0.87	4.00	1.0	-0.24	-0.20	4.09
HD 162396	0.83	4.20	1.5	-0.30	-0.25	4.28
HD 166913	0.84	3.90	1.6	-1.68	-1.46	4.33
HD 172167	0.53	4.00	2.0	-0.50	-0.33	4.29
HD 174912	0.86	4.30	1.0	-0.49	-0.42	4.42
HD 181743	0.85	4.20	1.2	-1.92	-1.71	4.47
HD 184499	0.89	4.00	1.0	-0.68	-0.59	4.18
HD 189558	0.89	4.00	1.1	-1.12	-0.93	4.35
HD 193307	0.85	4.20	1.0	-0.25	-0.22	4.27
HD 193901	0.89	4.00	1.0	-1.15	-0.97	4.37
HD 194598	0.85	4.10	1.0	-1.22	-1.06	4.38
HD 196892	0.85	4.00	1.1	-1.10	-0.92	4.32
HD 199289	0.86	4.00	1.0	-1.03	-0.86	4.28
HD 200973	0.80	3.90	1.0	-0.43	-0.36	4.01
HD 201099	0.87	4.10	1.0	-0.45	-0.39	4.20
HD 201889	0.90	4.00	1.2	-1.10	-0.94	4.24
HD 201891	0.86	4.40	1.0	-1.03	-0.87	4.74
HD 203608	0.83	4.40	0.9	-0.65	-0.57	4.54
HD 205294	0.81	4.00	1.0	-0.27	-0.21	4.13
HD 205650	0.87	4.00	1.1	-1.25	-1.03	4.38
HD 207978	0.80	4.00	1.0	-0.55	-0.45	4.17
HD 208906	0.85	4.00	1.0	-0.72	-0.58	4.20

TABLE 1—*Continued*

Star	$\Theta_{eff}$	logg(ETL)	v <sub>turb</sub> (km.s <sup>-1</sup> )	[Fe/H] <sub>(ETL)</sub>	[Fe/H] <sub>(NETL)</sub>	logg(NETL)
HD 210752	0.85	4.20	1.0	-0.60	-0.47	4.41
HD 211998	0.97	3.40	1.2	-1.48	-1.25	3.74
HD 213657	0.83	3.60	1.5	-1.97	-1.71	3.94
HD 215257	0.84	4.40	1.0	-0.55	-0.44	4.56
HD 215648	0.82	4.10	1.0	-0.28	-0.21	4.22
HD 216777	0.91	4.00	1.0	-0.70	-0.55	4.18
HD 218502	0.84	3.80	1.5	-1.75	-1.54	4.13
HD 218504	0.85	4.20	1.0	-0.54	-0.46	4.32
HD 221377	0.84	3.50	1.2	-1.20	-1.01	3.74
HD 222368	0.81	4.10	1.2	-0.12	-0.10	4.15
HD 224930	0.97	4.40	1.0	-0.80	-0.66	4.58
BD-13 3442	0.81	3.80	1.5	-3.00	-2.72	4.20
BD-10 388	0.86	3.30	1.4	-2.35	-2.04	3.71
BD-1 1792	1.01	3.00	1.0	-1.00	-0.84	3.27
BD-0 4234	1.06	4.20	1.0	-1.00	-0.82	4.38
BD 2 3375	0.87	3.80	1.2	-2.60	-2.29	4.22
BD 3 740	0.82	3.50	1.2	-2.80	-2.50	3.98
BD+17 4708	0.85	3.70	1.2	-1.75	-1.54	4.02
BD+23 3912	0.90	4.00	1.2	-1.67	-1.45	4.27
BD+26 3578	0.84	3.30	1.2	-2.35	-2.02	3.68
BD+29 366	0.91	3.80	1.2	-1.25	-1.07	4.10
BD+34 2476	0.82	4.00	1.2	-2.05	-1.80	4.34
BD+41 3306	1.05	4.00	1.2	-0.85	-0.70	4.19
CD-71 1234	0.80	4.30	1.0	-2.30	-2.05	4.56
CD-33 3337	0.85	3.60	1.5	-1.55	-1.35	3.91
CD-33 1173	0.79	4.00	1.5	-3.00	-2.69	4.39
CD-29 2277	0.86	4.50	1.0	-1.60	-1.38	4.76
G64-12	0.79	4.00	1.6	-3.35	-3.05	4.39
G275-4	0.84	4.00	1.5	-3.45	-3.12	4.39
CS22885-96	0.90	4.20	2.3	-4.20	-3.82	4.72
NLTT56-75	0.80	4.20	1.5	-2.70	-2.41	4.53
NLTT635-14	0.79	4.00	2.0	-2.45	-2.18	4.31
NLTT732-48	0.81	4.00	1.0	-2.35	-2.08	4.33
NLTT815-43	0.79	4.00	2.0	-2.95	-2.64	4.39
NLTT831-70	0.84	4.00	1.2	-3.15	-2.85	4.40
NLTT R740	0.92	3.20	1.5	-2.45	-2.16	3.67
SAO 27197	0.71	4.20	1.5	-0.52	-0.48	4.28
SAO 98468	0.72	4.20	1.5	-0.25	-0.24	4.28
SAO180920	0.76	4.20	1.0	-0.65	-0.57	4.33
NGC 752-218	0.75	3.60	3.8	0.00	0.00	3.60
SUN	0.87	4.44	1.0	0.00	0.00	4.44



**FIGURE 2**

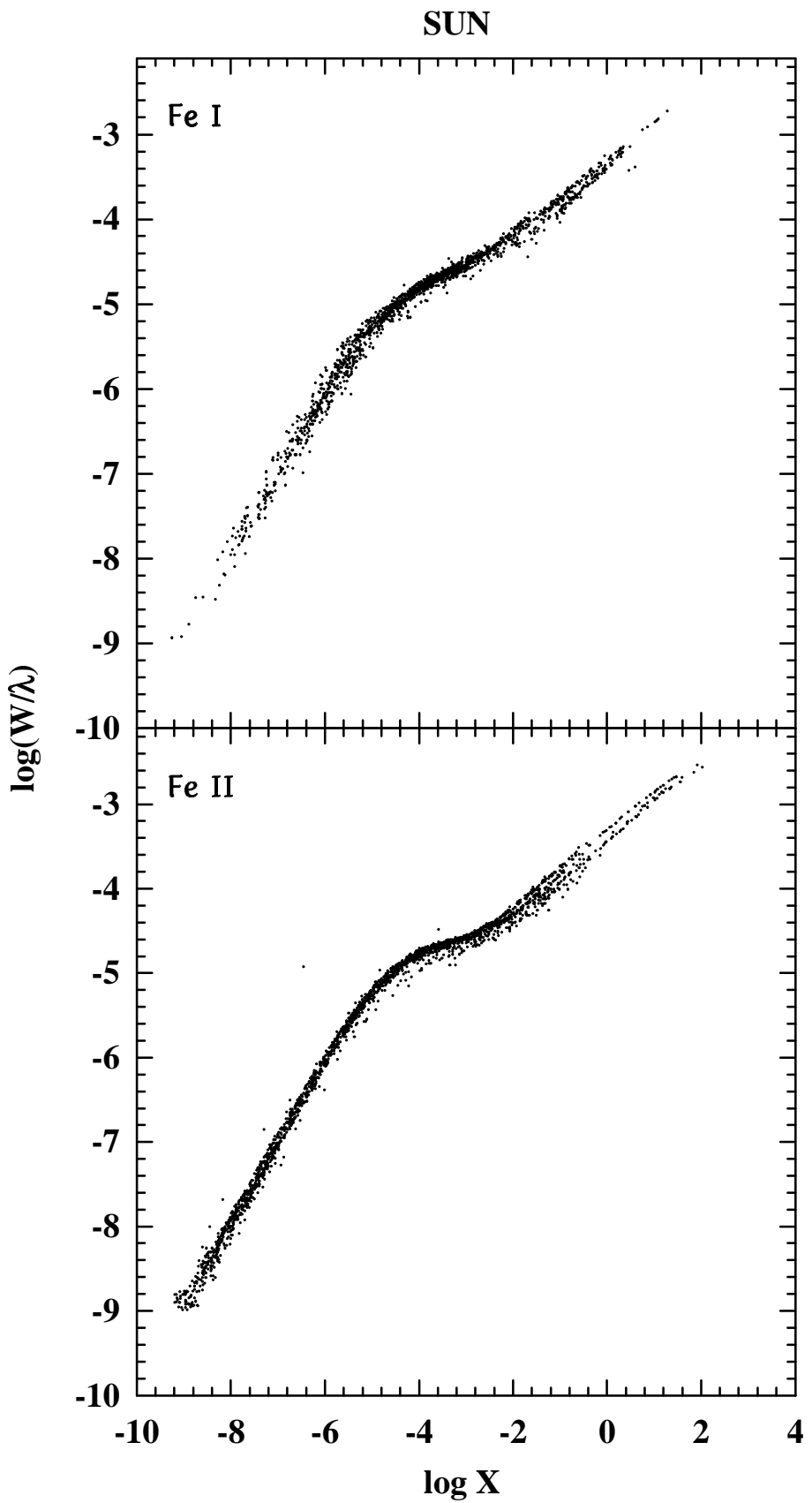
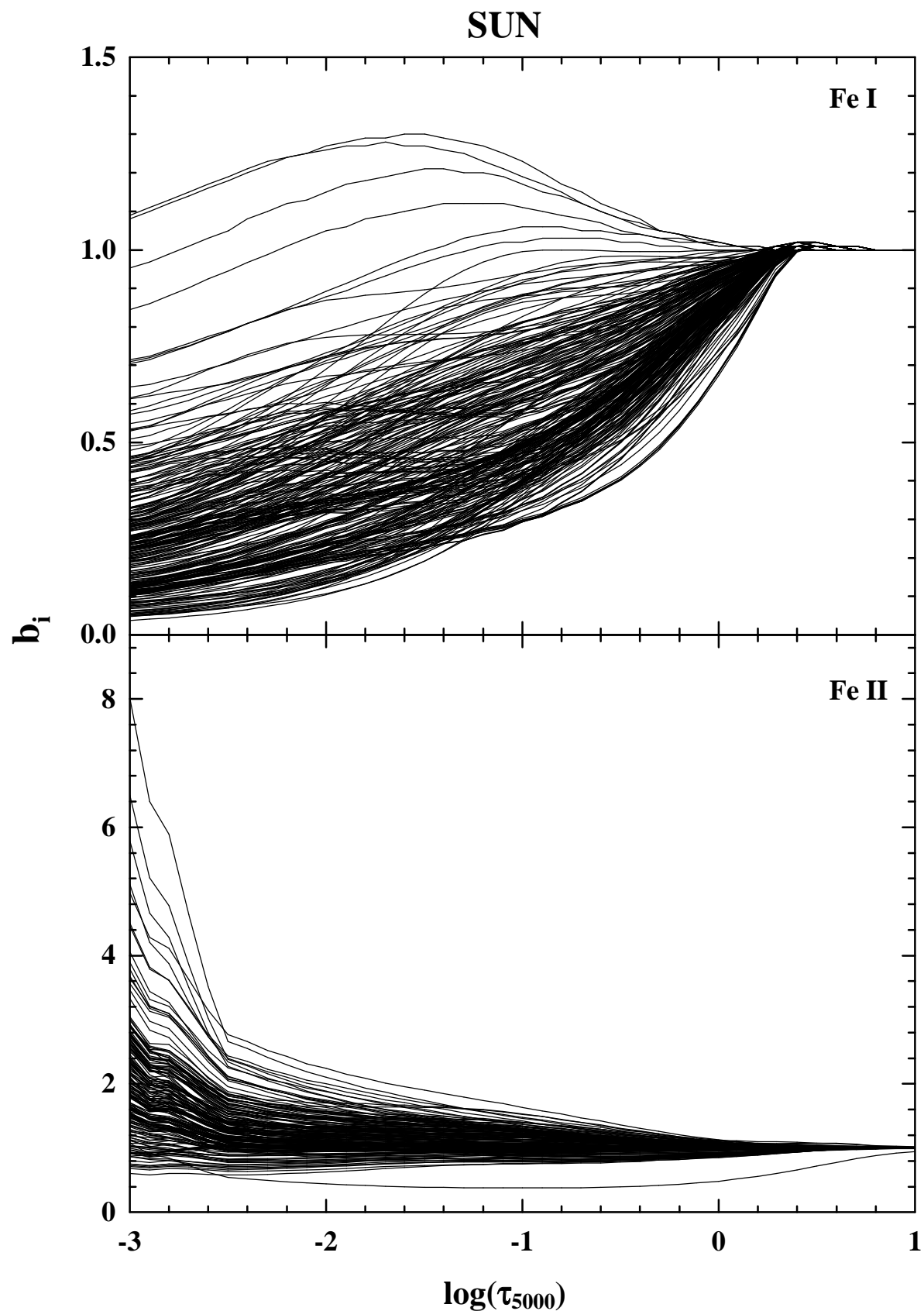
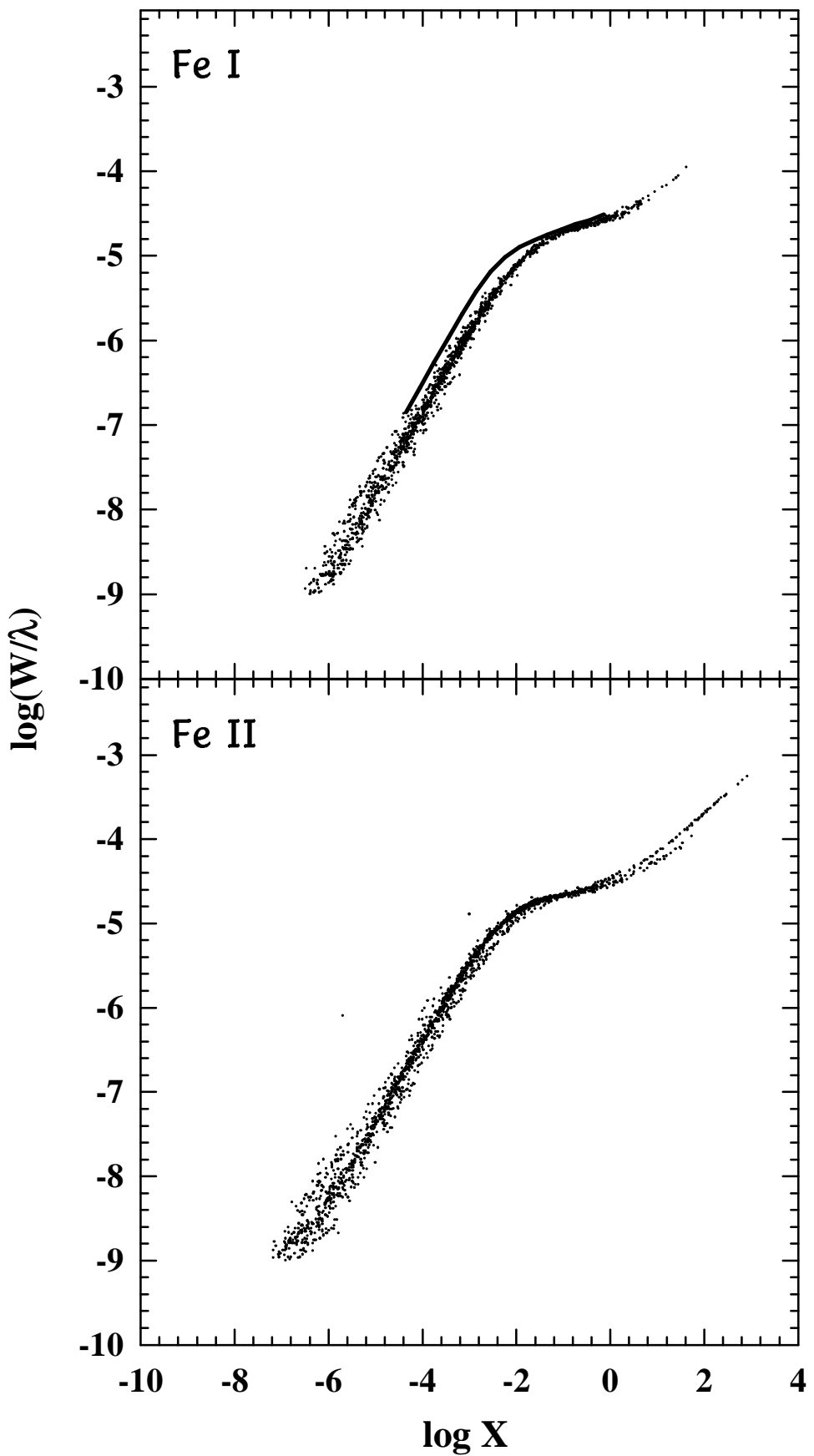


FIGURE 3



**FIGURE 4**



**FIGURE 5**

**HD 140283**

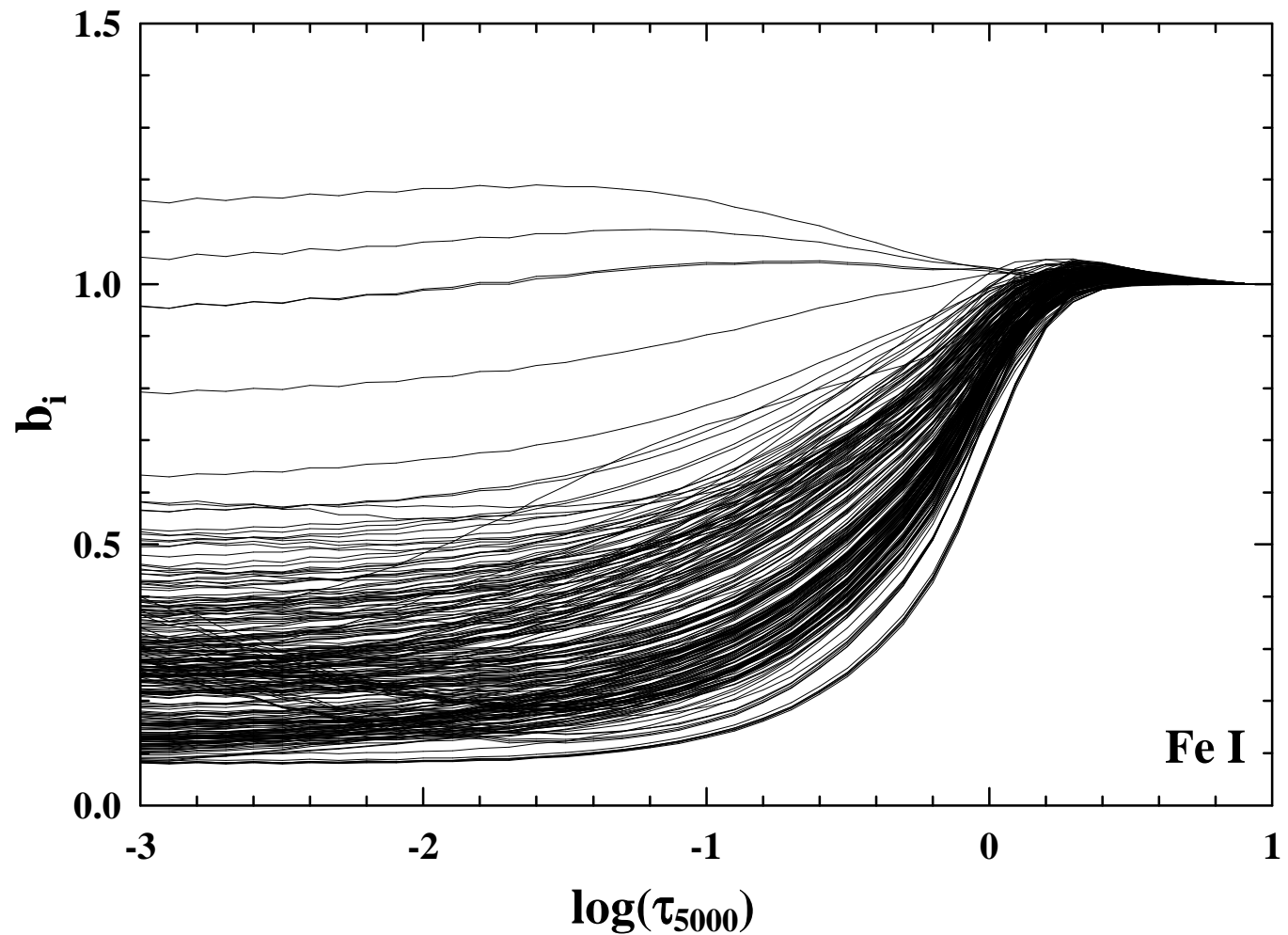


**FIGURE 6**

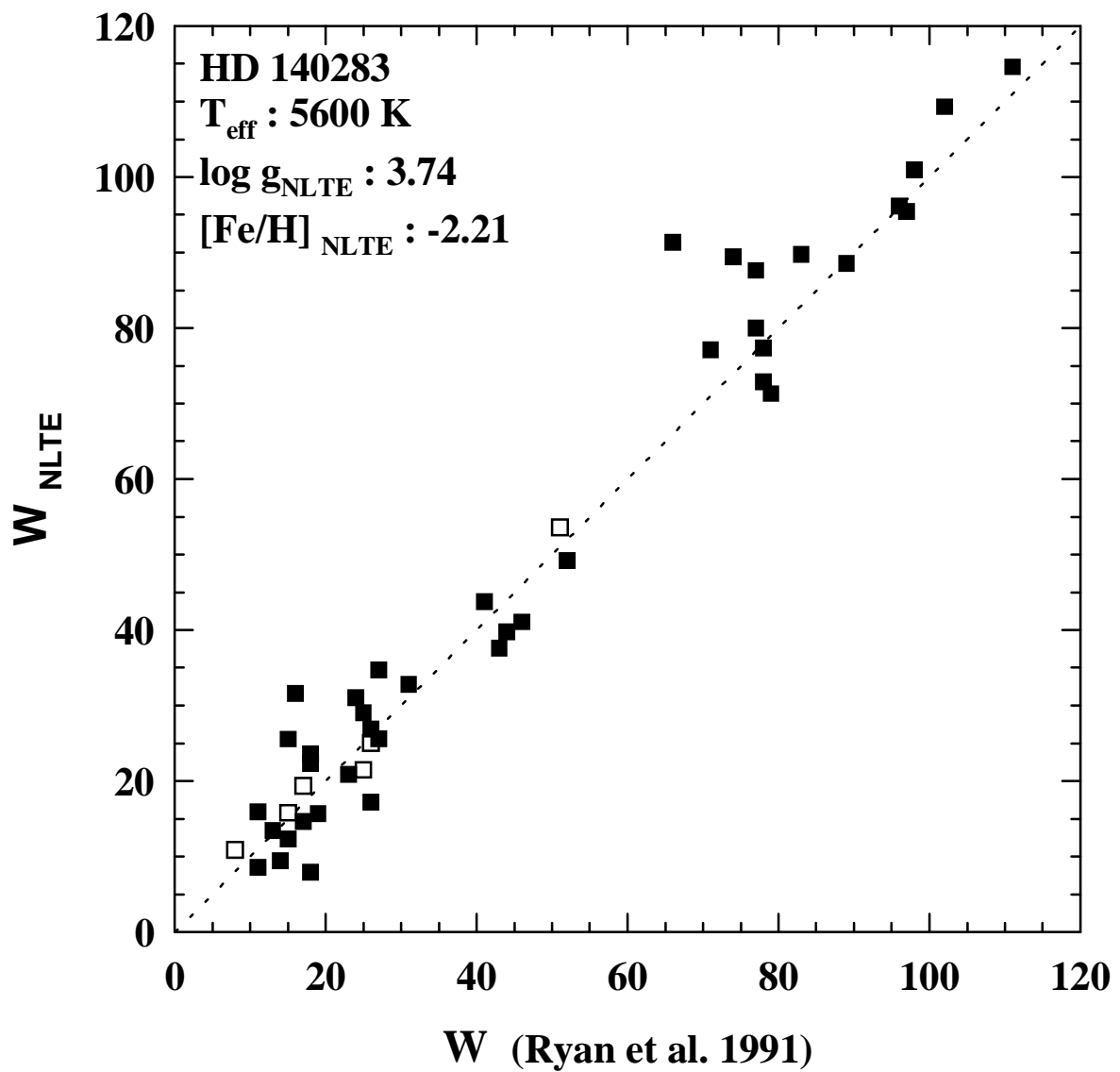


FIGURE 7

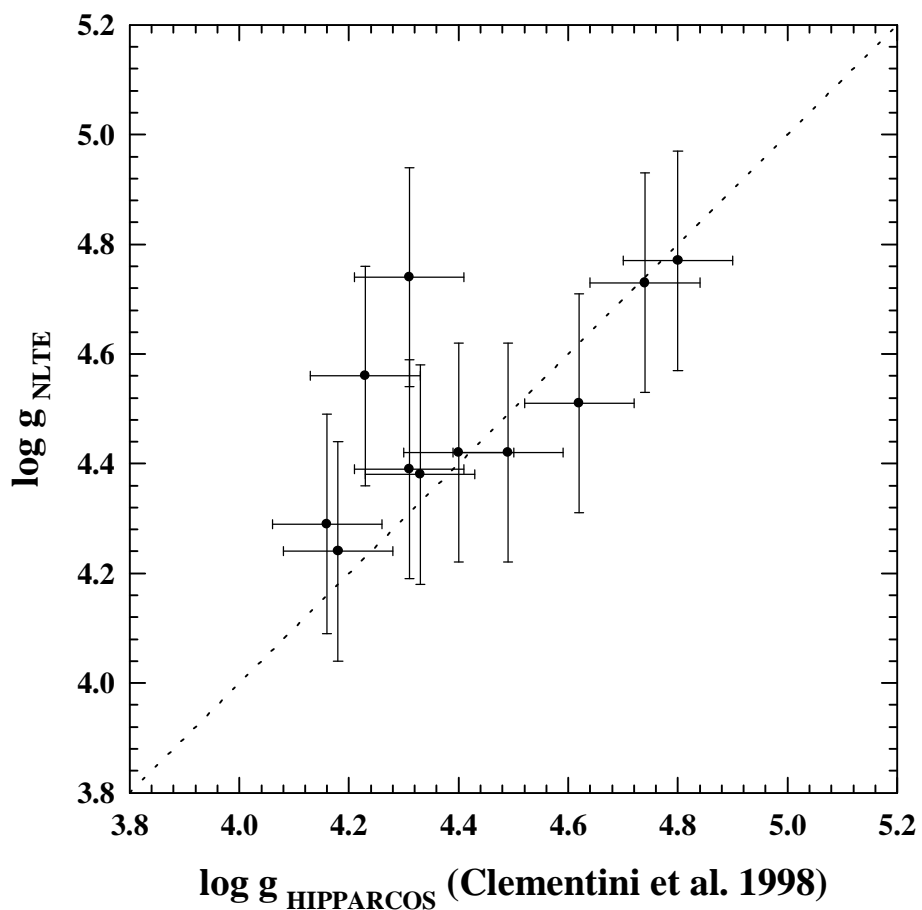
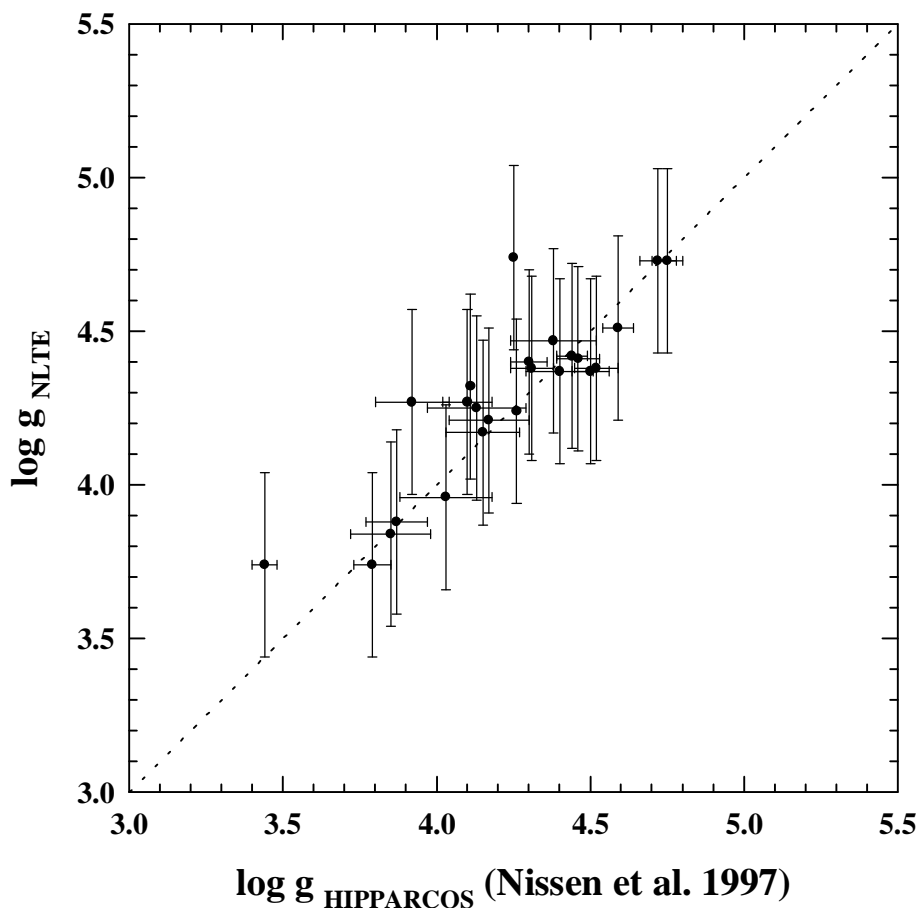
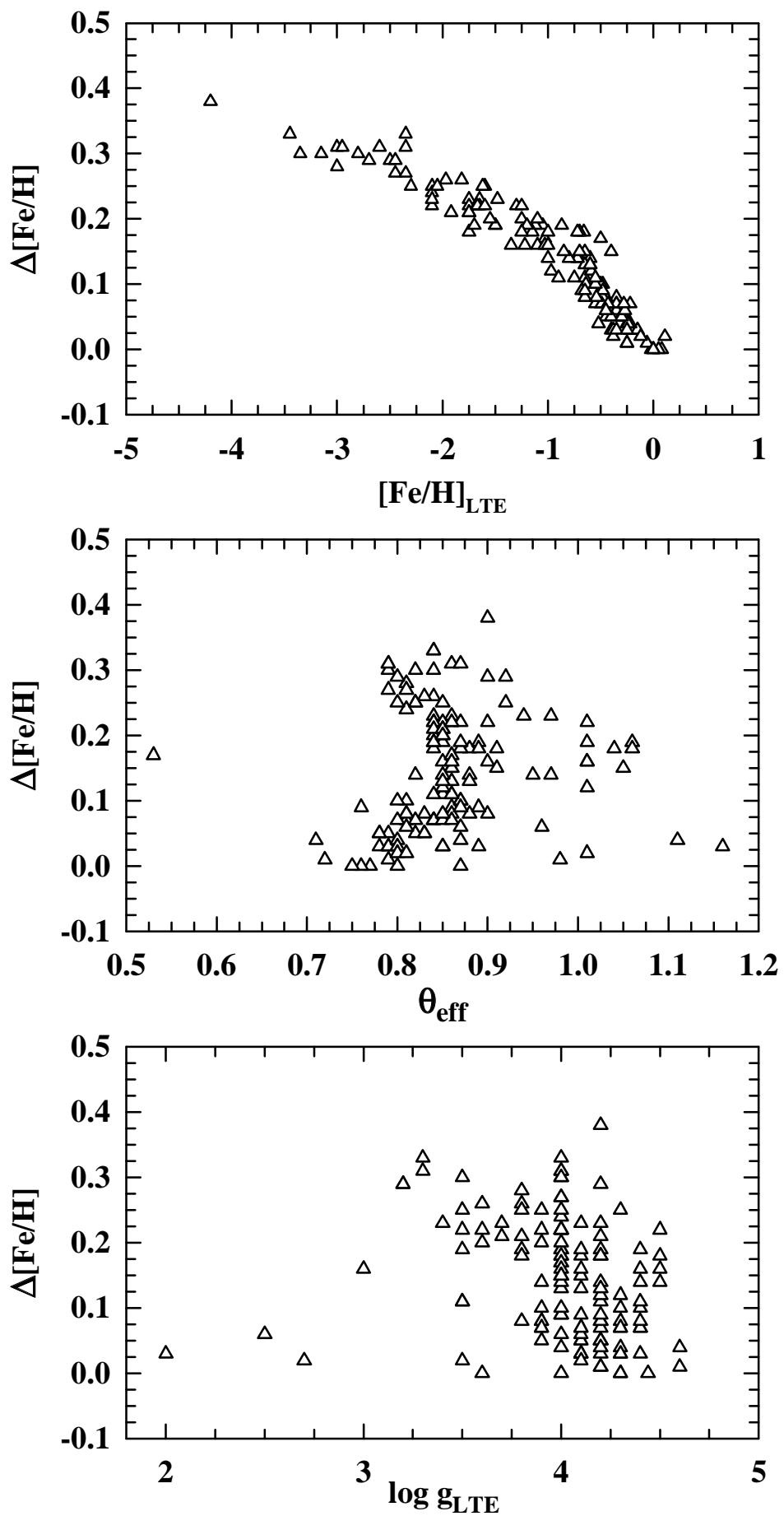


FIGURE 8



**FIGURE 9**